932 *Macromolecules* **2011**, *44*, 932–939
DOI: 10.1021/ma102156p

Macromolecules
ARTICLE

Rate-Dependent Stiffening and Strain Localization in Physically Associating Solutions

Kendra A. Erk and Kenneth R. Shull*

Department of Materials Science and Engineering, Northwestern University, 2220 Campus Drive, Evanston, Illinois 60208, United States

Received September 17, 2010; Revised Manuscript Received December 15, 2010

ABSTRACT: Model physically associating solutions of acrylic triblock copolymer molecules in a midblock-selective solvent displayed nonlinear strain-stiffening behavior which transitioned to rapid strain softening during shear start-up experiments at reduced rates spanning almost 4 orders of magnitude. Softening was believed to result from the shear-induced formation of highly localized regions of deformation in the macromolecular network. This behavior was accurately captured by a model that incorporated the strain energy and relaxation behavior of individual network strands in the solution. Flow curves predicted from the model were nonmonotonic, consistent with the onset of flow instabilities at high shear rates. The nonlinear stress response reported here, coupled with the wide range of accessible relaxation times of these thermoreversible solutions, makes them ideal model systems for studies of failure-mode transitions in physically associating solutions and gels.

1. Introduction

When soft polymeric materials are deformed in a nonlinear manner (e.g., to large strains or at high strain rates), the resulting mechanical behavior is commonly a function of the formation and evolution of a wide variety of instabilities, such as ductile and brittle fracture[1−3] and shear banding[4−6] in polymeric and micellar solutions and gels. There is much evidence to suggest that the type of instability developed in soft materials is strongly influenced by the structure of the material and the nature of the imposed deformation. This relationship between structure and deformation can be described by a reduced deformation rate, $\Gamma = \dot{\gamma}\tau$, defined as the product of the applied shear rate and the characteristic relaxation time of the material.[7] For $\Gamma \gg 1$, the material deforms more quickly than it can structurally rearrange to accommodate the applied stress and thus can be expected to behave elastically; for $\Gamma \ll 1$, the rate of relaxation is greater than the deformation rate and viscous-like behavior is expected.

Depending on the value of Γ, flow instabilities can form and evolve in different ways. These instabilities correspond to the development of a nonuniform strain rate throughout the thickness of a sample that is being sheared. Shear banding refers to the separation of the flow field into regions of different shear rates, corresponding to the existence of a kink in the velocity field. Fracture corresponds to the limiting case where a very high shear rate is obtained across a thin fracture plane. Sprakel et al.[8] have recently used particle-based simulations to investigate a "fracture-to-shear banding" failure-mode transition in transient polymer networks. Experimentally, Berret et al. have observed flow instabilities in aqueous telechelic polymer solutions,[7,9] and Hu et al. have observed similar behavior in entangled micellar solutions.[10] Tixier et al.[11] have seen rheological behavior consistent with a fracture-to-banding transition in networks formed from mixtures of surfactants and telechelic polymers.

A limitation of these previous experimental systems is that the relaxation times cannot be tuned over a range sufficient to access a broad spectrum of reduced rates. As a result, it is difficult to access behaviors well into both the low-Γ and high-Γ regimes without simultaneously changing structural features of the solutions such as the concentration of telechelic polymer molecules. Here, we utilize a model system with relaxation times that are strongly temperature dependent. Thus, an expanded window of accessible instabilities in the elastic ($\Gamma \gg 1$), viscoelastic ($\Gamma \sim 1$), and viscous ($\Gamma \ll 1$) regimes is achievable for these solutions. Shear start-up experiments were performed over a wide range of shear rates and temperatures such that Γ varied from 10^{-2} to 10^{2}. A constitutive model based on the macromolecular network structure of the solution was constructed and used to predict the nonlinear stress response of the solution during shear deformation and the corresponding flow curve.

2. Experimental Methods

2.1. Materials. The model physically associating solutions investigated here were composed of symmetric triblock copolymer molecules dissolved in a midblock-selective solvent. The triblock copolymer contained poly(methyl methacrylate) end blocks (PMMA; 8.9 kg/mol) separated by a poly(*n*-butyl acrylate midblock (PnBA; 53 kg/mol). Triblock copolymer was provided by Kuraray, Co. (Japan), and used as received. To form the physically associating solutions, copolymer was dissolved in 2-ethyl-1-hexanol (Sigma-Aldrich Co.; used as received) at temperatures above 80 °C in a magnetically stirred, sealed vial. The copolymer concentration in the solution was 5 vol %. The concentration was limited by the maximum applied torque of the rheometer; however, the chosen concentration was greater than the critical concentration corresponding to the network percolation threshold predicted by self-consistent mean-field theory.[12] The solution displayed a well-defined molecular structure which was characterized with small-angle X-ray scattering in a previous work.[13] Linear and nonlinear mechanical behavior was thoroughly investigated as well.[1,13,14]

The structure and mechanical properties of the physically associating solutions are dependent on temperature, as described in detail elsewhere.[14−16] In summary, at high temperatures (> 70 °C)

*Corresponding author. E-mail: k-shull@northwestern.edu.

 Published on Web 01/26/2011

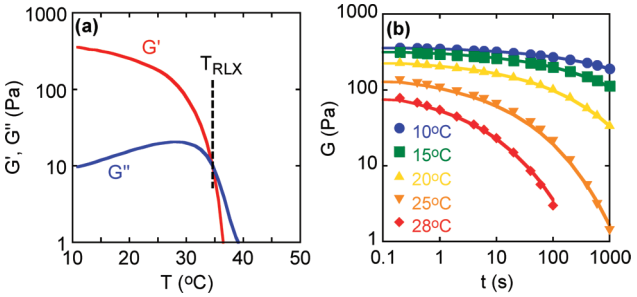

Figure 1. (a) Storage and loss modulus as a function of temperature for stress-controlled oscillatory measurements with σ = 10 Pa (linear regime) and ω = 10 rad s^{-1}. (b) Relaxation moduli at $T < T_{RLX}$ measured as a function of time for $\gamma_0 = 5\%$ (linear regime); solid lines correspond to stretched exponential fits from eq 1 with $\beta = 1/3$ as described in the following section.

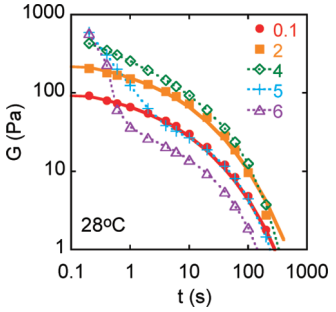

Figure 2. Relaxation moduli measured as a function of time at 28 °C for γ_0 = 10−600%. Solid curves are stretched exponential fits from eq 1 (G(0 s, 10%) = 140 Pa and G(0 s, 200%) = 330 Pa, τ = 2.4 s, β = 1/3). Dashed curves for $\gamma_0 \geq 400\%$ are to guide the eye during the accelerated relaxation.

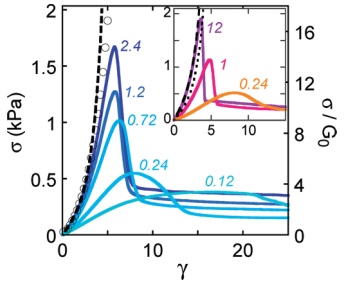

Figure 3. Representative nonlinear shear stress response of the physically associating solution. Main plot: response at 28 °C (τ=2.4 s) during shear start-up at 0.05−1.0 s^{-1} (Γ=0.12−2.4); dashed line indicates the predicted behavior in the elastic limit given by eq 2 with G_0 = 113 Pa and γ^* = 3.7 (ref 14); open symbols indicate the premaximum stress response during shearing at 5.0 s^{-1} (Γ=12), the highest shear rate investigated for a 28 °C solution. Inset plot: response during shear start-up at a fixed rate of 0.1 s^{-1} for a solution at 28 °C (Γ = 0.24), 25 °C (τ=10 s; Γ=1), and 20 °C (τ=120 s; Γ=12); elastic predictions from eq 2 with γ^* = 3.7 are shown by dashed line for 20 °C (G_0 = 264 Pa) and dotted line for 25 °C (G_0 = 167 Pa).

the triblock copolymer is fully dissolved in the solvent, forming a freely flowing, low-viscosity fluid. Below the critical micelle temperature (CMT; i.e., order−disorder transition), the PMMA end blocks self-assemble into spherical micelles or aggregates. Self-assembly of the network is driven by the temperature dependence of the interaction parameter between the solvent and the end blocks. The aggregates act as physical cross-links interconnected by dissolved PnBA midblocks; this network structure results in the formation of a viscoelastic liquid. As the solution is cooled toward the glass transition temperature of the partially solvated PMMA end blocks, the physical structure of the network remains unchanged. However, the exchange rate of PMMA end blocks between neighboring aggregates diminishes, and a strong, elastic material is formed. The concentration-dependent structural transition temperature between solid-like and liquid-like behavior is referred to as the relaxation temperature, T_{RLX}, which in practical terms can be viewed simply as the gelation temperature.[12]

2.2. Shear Rheometry. A stress-controlled Anton-Paar Physica MCR 300 (Ashland, VA) with Peltier temperature control was employed for all shear deformation experiments. Samples were contained in a single-gap Couette fixture (1.1 mm gap) with a fixture cover to prevent solvent loss. Samples were loaded in a fluid state, allowed to equilibrate for 5 min, and subsequently cooled and equilibrated at the temperature of interest. Step-strain and shear start-up experiments were performed to probe the linear and nonlinear mechanical behavior of the solution. The no-slip boundary condition between the solution and solid walls was verified optically with a particle tracking technique employing a Linkam CSS450 shear cell with parallel glass plates; for visualization purposes, samples were seeded with micrometer-sized polystyrene spheres. Full velocity profiles through the thickness of the deformed samples could not be obtained in our experiment. In the future, a more sophisticated flow-visualization technique, ideally employing a Couette cell with good temperature stability, could be used to quantify the local velocity profiles; such techniques are beyond our current experimental capabilities.

Because of the thermoreversibility of the samples and the temperature controls of the rheometer, one sample could be used for multiple shear start-up or step-strain experiments. After each experiment, the sample was heated to temperatures above T_{RLX} and allowed to rest in a low-viscosity fluid state for at least 5 min. After cooling and equilibrating at the temperature of interest, a new shear start-up or stress relaxation experiment could be performed, yielding identical results. Experimental results were found to be entirely reproducible and in agreement for one sample deformed multiple times, for different samples from the same batch of material, and for samples from different batches.

3. Experimental Results

The temperature-dependent mechanical response of the physically associating triblock copolymer solution is illustrated in Figure 1. The dynamic gelation temperature, T_{RLX}, between solid-like and liquid-like behavior was defined as the temperature at which the concentration-dependent characteristic relaxation time of the solution was on the order of 0.1 s as measured by oscillatory shear rheometry.[12,13] This transition roughly corresponded to the temperature at which G' and G'' were equivalent, i.e., the crossover point at ~34 °C in Figure 1a. In step-strain experiments (Figure 1b), the modulus decrease over time was indicative of stress relaxation taking place in the solution. Relaxation was accelerated as the temperature of the solution was increased toward T_{RLX}.

Step-strain experiments were performed with larger values of applied strain in order to probe the nonlinear viscoelastic response of the solution. Representative results are displayed in Figure 2 for values of applied strain from 10 to 600% at 28 °C. At γ_0 = 10%, linear relaxation behavior was observed. At $\gamma_0 > 10\%$, strain stiffening was seen, defined as an increase in $G(t \rightarrow 0\text{ s})$ with increasing values of applied strain. Above a critical value of applied strain, $\gamma_c \sim 400\%$, accelerated relaxation on the order of a few seconds was observed.

In shear start-up experiments, solutions were deformed at a range of fixed shear rates (0.02−5 s^{-1}) and temperatures (10−28 °C, $T < T_{RLX}$) in order to attain reduced rates of $\Gamma \approx 10^{-2}$−10^2. At 28 °C, the characteristic stress responses of both the low-Γ *and* high-Γ regimes were observed within the experimentally accessible range of shear rates (see main plot of Figure 3). Similar Γ-dependent behavior was also observed for solutions deformed

at a fixed shear rate and range of temperatures (see inset of Figure 3). The nearly identical curves for $\Gamma = 0.24$ in the main and inset plots of Figure 3 were measured for two different samples of solution at the same experimental conditions (0.1 s^{-1} and 28 °C), indicating the strong reproducibility of the nonlinear response.

At shear rates such that $\Gamma > 1$ for the 28 °C solutions (main plot of Figure 3), strain-stiffening behavior was clearly observed followed by a maximum in the stress response occurring at ~600% strain. At lower shear rates ($\Gamma < 1$), the maximum in the stress−strain curve persisted, although shifting to greater values of strain. Another notable feature of Figure 3 is the existence of nonzero stress plateaus following the stress maximum. Stress maxima and postmaximum stress plateaus were present for all reduced rates investigated here, $\Gamma = 0.048-330$.

The representative Γ-dependent stress responses shown in Figure 3 illustrate the primary nonlinear signatures observed for these physically associating solutions deformed in shear at $T < T_{RLX}$: (1) strain stiffening due to network strand stretching at relatively low values of strain; (2) strain softening due to breakdown or fracture of the macromolecular network at intermediate values of strain. These experimental results and conclusions are discussed in the following sections. The finite values of stress at large strain are believed to be due to frictional stresses at the network's failure interface; this behavior will be discussed in a future publication.

4. Discussion of Experimental Results

4.1. Linear Temperature-Dependent Behavior. The self-assembled structure and corresponding mechanical response of the physically associating triblock copolymer solution are a strong function of temperature. The thermoreversible self-assembly of the physical network is driven by the temperature dependence of the interaction parameter between the solvent and the end blocks.[16] For the PMMA/alcohol system, this temperature dependence is unusually strong within the experimentally accessible temperature window, leading to the mechanical response displayed in Figure 1a. For $T < T_{RLX}$, the solution behaves in an elastic manner with $G' \gg G''$. This elasticity is due to the interconnected macromolecular network of rubbery midblock strands and end block aggregates. At lower temperatures such as 10 °C ($T \ll T_{RLX}$), the end block segments apparently become "frozen" or kinetically trapped in the glassy aggregates,[17] preventing chain pull-out and forming an elastic, macromolecular network with extremely long relaxation times as shown in Figure 1b.

As the temperature of the solution is increased toward T_{RLX}, the response of the network changes from purely elastic to viscoelastic, with G'' increasing relative to G' as shown in Figure 1a. At these intermediate temperatures, relaxation times became shorter and stress relaxation is accelerated. Stress relaxation most likely occurs by the exchange of end block segments between neighboring aggregates in the physical network.[18] As the temperature is further increased above the dynamic gelation temperature, physical cross-links are created and annihilated rapidly, resulting in the formation of a freely flowing, viscous liquid.[19,20]

The linear relaxation behavior of the physically associating solutions can be modeled by a stretched exponential function, suggested to describe relaxation in complex, strongly interacting materials[21] and used previously to describe a variety of polymer networks and gels, including transient telechelic networks[22] and symmetric triblock copolymer melts:[23]

$$G(t,\gamma_0) = G(0,\gamma_0)\exp\left[-\left(\frac{t}{\tau}\right)^{\beta}\right], \quad 0<\beta<1 \qquad (1)$$

where $G(0,\gamma_0)$ is the relaxation modulus extrapolated to zero time, τ is the apparent viscoelastic relaxation time in the small-strain regime, and β describes the width of the relaxation time distribution ($\beta = 1$ indicates a single relaxation time[21]). The solid lines in Figure 1b correspond to eq 1 with the input parameters reported in Table 1. The relaxation behavior is accurately described by $\beta = 1/3$ between 10 to 28 °C, a temperature range over which τ is found to decrease from 3300 to 2.4 s. Interestingly, this value of 1/3 for β is characteristic of the behavior of a range of complex fluids,[24,25] suggesting that our model system is a useful model for a broader class of soft material systems.

Table 1. Parameters Used in eq 1 To Describe the Stress Relaxation Behavior of the Physically Associating Solution over a Range of Temperatures

T (°C)	$G(0)$ (Pa)[a]	τ (s)
10	373	3300
15	338	700
20	264	120
25	167	10
28	113	2.4

[a] $G(0)$ given by $G'(\gamma_0 = 5\%, \omega = 100$ rad $s^{-1})$ at each temperature.

4.2. Strain-Stiffening Behavior. Evidence of nonlinear, strain-stiffening behavior was observed during step-strain experiments (Figure 2) as well as shear start-up experiments (Figure 3). Strain stiffening of these solutions in the elastic regime (i.e., at $T \ll T_{RLX}$, where $\Gamma \gg 1$) has been discussed in detail previously[14] and is summarized briefly here. The following constitutive equation was found to accurately describe the stiffening behavior of physically associating networks of triblock copolymers solutions as well as various biopolymer networks:[14]

$$\sigma = G_0\gamma\exp\left[\left(\frac{\gamma}{\gamma^*}\right)^2\right], \quad \text{for } \Gamma \gg 1 \qquad (2)$$

where G_0 is the small-strain shear modulus and γ^* is the only adjustable parameter needed to describe the strain-stiffening behavior. Here, σ is used to denote shear stress in order to avoid confusion with the symbol used for relaxation time, τ. The critical value of strain, γ^*, is the value of strain at which stress divergence occurs due to strain-stiffening effects. This critical strain was found previously to increase with the molecular weight of the midblock segment, implying that strain stiffening was ultimately controlled by the finite extensibility, and thus the overall length, of a compliant strand in the macromolecular network.[14]

The dashed and dotted lines in Figure 3 show the elastic stiffening response predicted for 20, 25, and 28 °C solutions by eq 2 with $G_0 \approx G(0)$ from Table 1 and $\gamma^* = 3.7$, the characteristic critical strain for the triblock copolymer network investigated here.[14] At 20 °C ($\Gamma = 12$ in the inset of Figure 3), the stiffening behavior of the solution nearly matches the elastic prediction. At higher temperatures, the solutions behaved as viscoelastic materials with Γ closer to unity, and as shown in Figure 3, strain stiffening is still observed for these solutions. However, the overall magnitude of stiffening was reduced from the predicted elastic responses for the 25 and 28 °C solutions, even for the highest shear rate investigated at 28 °C

(shown as open symbols in the main plot; higher shear rates could not be investigated for this solution due to the torque limitation of the rheometer). Additionally, the stiffening magnitude was further decreased at lower deformation rates; this reduction is clearly seen by comparing $\Gamma = 2.4$ and $\Gamma = 1.2$ to the dashed line in the main plot of Figure 3. Thus, in the viscoelastic regime, stress relaxation seems to occur in the solutions well before the stiffening limit can be reached, leading to an overall reduction in the stiffening magnitude from the predicted elastic response.

4.3. Rate-Dependent Mechanical Instability. In addition to strain stiffening, Figures 2 and 3 display a second regime of nonlinearity at larger values of strain. For the step-strain experiment shown in Figure 2, above a critical value of applied strain, $\gamma_c \sim 400\%$, accelerated relaxation was observed. Similar two-step relaxation behavior has been observed previously in telechelic polymer networks[22] and was attributed to two populations of elastically active chains: (1) highly stretched chains that rapidly dissociate from the network junctions and relax and (2) less stretched chains that relax within the typical network time. Evidence of a critical value of strain was also seen in shear start-up experiments (main plot of Figure 3), where the observed strain-stiffening behavior transitioned to strain softening above ~400% strain. Thus, we suggest that the strain softening at $\gamma > \gamma_c$ is most likely due to damage accumulation in the solution as highly stretched network strands dissociate from their respective network junctions and relax.

For solutions deformed in shear at $\Gamma > 1$, rapid strain softening was observed at strains near 600% (main plot of Figure 3). Similar shear stress maxima have been observed elsewhere by Berret et al.[7,9] in the shear-thinning regime of aqueous telechelic polymer solutions and by Skrzeszewska et al.[26] for telechelic polypeptides; in these studies, the stress maxima were demonstrated by particle image velocimetry, a flow visualization technique, to be due to the formation of a fracture zone within the sample.[9,26] In our solutions, deformation energies of 3−4 J m^{-2} were estimated from integration of the stress maxima at the highest shear rates. These values are consistent with fracture energies obtained from conventional mode I fracture tests of similar acrylic triblock copolymer gels.[1] On the basis of these similarities and the damage accumulation observed at $\gamma > 400\%$ in step-strain experiments, we believe that the rapid strain softening taking place in our solutions for $\Gamma > 1$ is an indication of shear-induced breakdown of the macromolecular network.

It is also worth noting that the value of strain corresponding to the rapid softening behavior at $\Gamma > 1$ in our solutions was very weakly dependent on the applied shear rate. This is consistent with the fluid fracture experiments of Berret et al.[9] and with more recent theoretical results and start-up experiments of nonlinear stress growth in telechelic polymer solutions[27] and more complex transient networks.[4]

At lower reduced rates ($\Gamma < 1$), the maxima in the stress−strain curves persisted, although the feature shifts to greater values of strain. The stress maximum for the $\Gamma = 0.24$ case occurs ~80 s after shear inception, a time on the order of 30τ for the solution. Similar slow relaxation behavior was observed by Berret et al.[7] for telechelic solutions deformed at $\Gamma < 1$; steady-state behavior was only reached after $t \gg \tau$ and for deformations up to several hundred strain units. These slow relaxations at the onset of the shear thinning regime were suggested by the authors to be similar to the long-time relaxations of worm-like micelles in shear flow,[28−30] which are related to the nucleation and growth of macroscopic shear bands.[31]

5. Molecular Origins of the Rheological Response

In order to elucidate the structure−property relationship in our solutions, we have constructed a constitutive model to predict the stress response of the solution based on the evolution of the physically associating macromolecular network during the deformation process. In brief, the overall stress response of the solution is calculated from the deformation-dependent concentration of elastically active triblock copolymer strands in the macromolecular network, fundamentally similar to theory proposed recently by Tripathi et al.[32] In the following subsections, we introduce the physical assumptions of our model, the method of solution, and the resulting predictions and implications of the model.

5.1. Constitutive Model. We begin with an expression for the bulk elastic strain energy density, U, that is stored in the physically associating solution as it deforms:

$$U = \frac{G_0}{2} J^* \left[\exp\left(\frac{J_1}{J^*}\right) - 1 \right];$$
$$J_1 = \lambda_1^2 + \lambda_2^2 + \lambda_3^2 - 3 \quad (3)$$

where G_0 is the small-strain shear modulus and λ_1, λ_2, and λ_3 are the principal extension ratios. At small strains, this expression reduces to the neo-Hookean model. At larger strains, the finite extensibility of the network strands and the subsequent strain-stiffening behavior are accurately described by a single fitting parameter, J^*. This expression has been employed previously to describe the large strain behavior of elastic, self-assembled triblock copolymer gels deformed in uniaxial compression[1] and shear[14] and equivalent functions have been applied to describe the nonlinear elasticity of biological systems[33] and recently stiff polymer networks.[34] The physically associating solution is assumed to deform affinely, so that the local extension ratios describing the deformation of individual network strands are equal to the macroscopic extension ratios. Assuming an incompressible material ($\lambda_1^2\lambda_2^2\lambda_3^2 = 1$) undergoing shear deformation in the 1−2 plane ($\lambda_3 = 1$), eq 3 can be modified to yield the shear stress as a function of shear strain for a strain-stiffening solution. This relationship is obtained by noting that the shear strain, γ, is given by $\lambda_1 - \lambda_2$, so that $J_1 = \gamma^2$. Equation 2 for the shear stress is obtained from the condition that $\sigma = dU/d\gamma$, recognizing that $J^* = (\gamma^*)^2$.

We assume that strain energy is stored in deformed network strands or "bonds", which in our case correspond to bridging midblocks that span different end block aggregates. In a dynamic system like the triblock solutions used in our experiments, molecules are constantly transforming from these load-bearing "bridging" configurations to non-load-bearing "looping" configurations, where both end blocks reside in the same aggregate. In the undeformed state at equilibrium, the concentration of load-bearing bonds is given by the quantity $f_0\nu$, where f_0 is the equilibrium bridging fraction and ν is the overall concentration of triblock copolymer molecules. For a purely elastic system, the resulting shear modulus must be proportional to the bond concentration and to U_b, the strain energy per bond. As a result, we can write the following expressions for G_0 and U_b for the elastic case:

$$U = f_0\nu U_b, \quad G_0 = Ck_BTf_0\nu \quad (4)$$

where C is a dimensionless constant of order unity that involves factors such as the swelling of the network strands.[35]

In mathematical terms, our assumption of affine deformation means that it is possible to define a quantity J_{1b} that

describes the state of strain for an individual bond and that U_b is related to J_{1b} by an expression with the same form as eq 3. The correct prefactor is obtained by the requirement that the expressions in eq 4 be recovered, leading to the following for U_b:

$$U_b = \frac{G_0}{2f_0\nu} J^* \left[\exp\left(\frac{J_{1b}}{J^*}\right) - 1\right] \tag{5}$$

The stress contribution of each bond is obtained by the appropriate derivative of this strain energy function. While this procedure can be generalized to arbitrary strain states, we focus here on the case of simple shear, where the individual bond strains are specified by the local shear strain, γ_b. In this case, $J_{1b} = {\gamma_b}^2$ and we obtain a "stress per bond", σ_b, that is related to γ_b by what can be viewed as a molecular-scale version of eq 2:

$$\sigma_b = \frac{dU_b}{d\gamma_b} = \frac{G_0\gamma_b}{f_0\nu} \exp\left[\left(\frac{\gamma_b}{\gamma^*}\right)^2\right] \tag{6}$$

For a completely elastic system, the bond strains in an affinely deformed network are all assumed to be equal to the macroscopic strain. However, in a viscoelastic system where some of the bond strains can be relaxed by pullout of the end blocks from the aggregates in which they are embedded, a range of bond strains will exist because pullout is assumed to "reset" the strain in that particular bond to zero. In this case we need to introduce a bond strain distribution function, $\phi_b(t,\gamma_b)$, where $\phi_b(t,\gamma_b)\, d\gamma_b$ is the probability that a given bond has a strain between γ_b and $\gamma_b + d\gamma_b$ at time t. The macroscopic shear stress is obtained by integrating over the contributions from all possible values of the bond strain:

$$\sigma(t) = \nu \int_{-\infty}^{\infty} \sigma_b(t,\gamma_b)\phi_b(t,\gamma_b)\, d\gamma_b \tag{7}$$

The specific case of relevance to our experiments involves the imposition of a constant strain rate, $\dot{\gamma}$, beginning at $t = 0$. Individual bond strains are assumed to increase at a rate equal to the macroscopically imposed strain rate, so the range of possible bond strains is from 0 to γ, with γ being the macroscopic strain. Under these conditions we can use γ as the independent variable, and eqs 6 and 7 combine to give the following:

$$\frac{\sigma(\gamma)}{G_0} = \frac{1}{f_0}\int_0^{\gamma} \phi_b(\gamma,\gamma_b)\gamma_b \exp\left(\frac{\gamma_b}{\gamma^*}\right)^2 d\gamma_b \tag{8}$$

At this point the problem is reduced to the development of a physically meaningful expression for the time dependence (and subsequent strain dependence) of the bond strain distribution function, ϕ_b. As with the strain-stiffening function, the existing experimental data provide some guidance in this area. At low strains, the stress relaxation function is determined by the rate at which individual bonds are broken. For relatively low values of the applied strain, we use the following bond survival probability, $p_b(t')$, that is consistent with the stress relaxation data shown in Figure 1b:

$$p_b(t') = \exp\left[-\left(\frac{t'}{\tau}\right)^{\beta}\right] \tag{9}$$

Here, t' is the bond lifetime—the time since a given bond was last fully relaxed. An additional factor that must be accounted for is that the relaxation time, τ, must itself depend on the bond stress or, equivalently, on the bond strain γ_b. We see experimental evidence of this in Figure 2, as

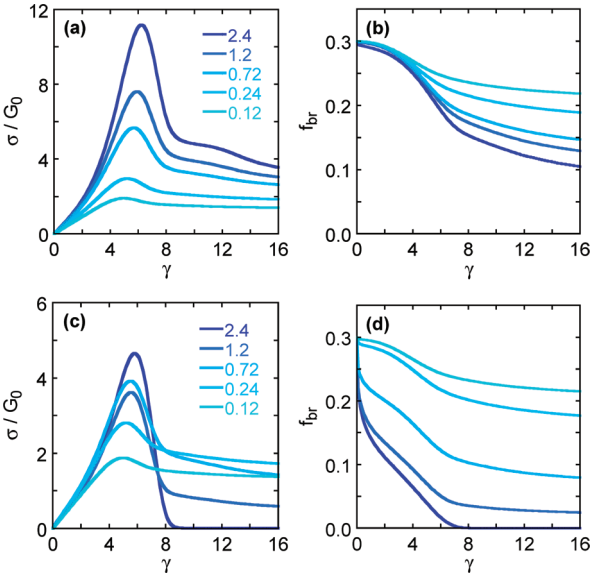

Figure 4. (top) Model predictions for $\Gamma \ll \Gamma^*$: (a) normalized macroscopic stress and (b) overall bridging fraction as a function of strain for reduced rates of 0.12−2.4 with $\Gamma^* = 10$. (bottom) Predictions for $\Gamma \geq \Gamma^*$: (c) normalized macroscopic stress and (d) overall bridging fraction as a function of strain for reduced rates of 0.12−2.4 with $\Gamma^* = 1$. The following parameters are used: $f_0 = 0.3$, $\gamma_f = 2.9$, $\beta = 0.33$, and $\gamma^* = 3.7$.

accelerated relaxation is observed in the solution for greater values of applied strain. Previous models developed by Tanaka and Edwards,[36] Michel et al.,[37] and Sprakel et al.[38] rely on a simple exponential relationship (i.e., $\beta = 1$) between the bridge lifetime and the deformation-induced elastic restoring force. While a variety of forms can be used, we use the following simple expression for the evolution of the relaxation time with bond strain, squared to account for the equivalence of positive and negative values of the shear strain:

$$\tau(\gamma_b) = \tau_0 \exp\left[-\left(\frac{\gamma_b}{\gamma_f}\right)^2\right] \tag{10}$$

where γ_f can be viewed as a characteristic fracture strain.

Equation 10 applies to the situation where the strain is instantaneously increased to γ_b and fixed at this level, whereas in reality the bond strains are increasing at a fixed rate. The situation can be simplified by defining the following effective bond lifetime, t_{eff}:

$$t_{eff} = \int_0^{t'} \exp\left(\frac{\gamma_b}{\gamma_f}\right)^2 dt \tag{11}$$

For shear deformation at a constant strain rate, $t' = \gamma_b/\dot{\gamma}$, and thus

$$t_{eff} = \frac{1}{\dot{\gamma}}\int \exp\left(\frac{\gamma_b}{\gamma_f}\right)^2 d\gamma_b = \frac{\pi^{1/2}}{2\dot{\gamma}}\gamma_f \,\mathrm{erfi}\left(\frac{\gamma_b}{\gamma_f}\right) \tag{12}$$

where erfi is the imaginary error function. For a shear start-up experiment we can replace the bond lifetime t' in eq 9 with this effective lifetime. By introducing the reduced rate, $\Gamma = \dot{\gamma}\tau$, we obtain the following expression for the bond survival probability:

$$p_b(\gamma_b) = \exp\left[-\left(\frac{\pi^{1/2}}{2\Gamma}\gamma_f \,\mathrm{erfi}\left(\frac{\gamma_b}{\gamma_f}\right)\right)^{\beta}\right] \tag{13}$$

Equation 13 gives the probability that a given bond survives to reach a strain of γ_b, assuming that the system is being deformed at a constant value of Γ. In order to determine the full strain dependence of ϕ_b, we need to specify the fate of the bonds that do not survive. In our triblock copolymer system, these broken bonds correspond to PMMA end blocks that have pulled out of their original aggregate and are inserted into a different aggregate. Some fraction of these end blocks form loops, with both PMMA blocks attached to a given midblock residing in the same PMMA aggregate. The remaining midblocks are assumed to form bonds with a bond strain that is "reset" to zero. At low strain rates, corresponding to small values of Γ, the fraction of midblocks that form new bonds is given by the equilibrium bridging fraction, f_0. For higher strain rates, the continuous deformation imposed by the shear field will make bridge formation less likely. The detailed functional form of the decrease in bridging fraction with increasing strain rate does not significantly affect the model predictions. For simplicity, we use the following function to describe the fraction of broken bonds that are reset to bridges:

$$f_{br} = f_0 \exp\left[-\left(\frac{\Gamma}{\Gamma^*}\right)^2\right] \tag{14}$$

Because of the dynamic nature of the system, we must also consider the transformation of loops into bridges. Because loops do not experience any stress in our model, they have a relaxation behavior that is assumed to be independent of the strain rate. In order to maintain an equilibrium bridging fraction at vanishingly small strain rates, the loop survival probability, p_l, must have a form that is equivalent to eq 9. To handle loops and bridges in a consistent way, it is helpful to define an effective loop strain, γ_l, given by $\gamma_l = t'\dot{\gamma}$, so that p_l is given by the following expression:

$$p_l(\gamma_l) = \exp\left[-\left(\frac{\gamma_l}{\Gamma}\right)^\beta\right] \tag{15}$$

Because loops do not contribute to the stress, the definition of an artificial loop strain in this way does not affect the results of the model.

5.2. Method of Solution. The physical approximations included in our model are embedded in the equations given in the previous section. Here we provide some additional information to illustrate the way in which these equations are implemented into our complete numerical solution. We begin by defining separate strain distribution functions $\phi_{b0}(\gamma)$ and $\phi_{l0}(\gamma)$, such that $\phi_{b0}(\gamma)\,d\gamma$ and $\phi_{l0}(\gamma)\,d\gamma$ are the respective fractions of the triblock copolymer molecules that have been reset into bridges and loops at macroscopic strains between γ and $\gamma + d\gamma$. At the outset of the deformation, $\phi_{b0}(\gamma)$ and $\phi_{l0}(\gamma)$ are given by the equilibrium bridging fraction:

$$\phi_{b0} = f_0\delta(\gamma), \quad \phi_{l0} = (1-f_0)\delta(\gamma) \tag{16}$$

where $\delta(\gamma)$ is the Dirac delta function. At a point in time when the macroscopic strain is equal to γ, bonds with a strain of γ_b were formed when the macroscopic strain was equal to $\gamma - \gamma_b$. The actual strain distribution functions are obtained by multiplying by the appropriate bond and loop survival probabilities:

$$\begin{aligned}\phi_b(\gamma,\gamma_b) &= \phi_{b0}(\gamma-\gamma_b)p_b(\gamma_b),\\ \phi_l(\gamma,\gamma_l) &= \phi_{l0}(\gamma-\gamma_l)p_l(\gamma_l)\end{aligned} \tag{17}$$

The strain distribution functions are defined so that they are normalized for any given value of γ. This requirement that the distributions functions remain normalized provides a means for calculating the evolution of ϕ_{b0} and ϕ_{l0} as γ increases. Suppose for example that we know the values of these quantities at some value of γ. At $\gamma + \Delta$, where Δ is a small increment to the macroscopic strain, we have

$$\begin{aligned}&\Delta(\phi_{b0}(\gamma+\Delta)+\phi_{l0}(\gamma+\Delta))\\ &= 1-\int_0^\gamma \phi_{b0}(\gamma-\gamma_b)p_b(\gamma_b+\Delta)\,d\gamma_b\\ &\quad -\int_0^\gamma \phi_{l0}(\gamma-\gamma_l)p_l(\gamma_l+\Delta)\,d\gamma_l\end{aligned} \tag{18}$$

The relative magnitudes of $\phi_{b0}(\gamma + \Delta)$ and $\phi_{l0}(\gamma + \Delta)$ are determined by eq 14. Beginning with the initial condition of eq 16, we successively increment γ, using eq 18 to generate the complete relationship between ϕ_{b0}, ϕ_{l0}, and the macroscopic strain. Once these relationships are obtained, we use eqs 8, 13, and 17 to obtain the evolution of the macroscopic stress in the system.

5.3. Model Predictions and Implications. Figure 4 shows the normalized stress predictions for reduced rates of $\Gamma = 0.12-2.4$ for two different scenarios: $\Gamma \ll \Gamma^*$ and $\Gamma \geq \Gamma^*$, where Γ^* is the critical reduced rate where the bridge-to-loop transition occurs. In each case, we use a value for γ_f of 2.9 in order to obtain results that are consistent with the experimental data in Figure 3. The equilibrium bridging fraction was found to be ~0.3 from self-consistent mean-field simulations.[12] The results for $\Gamma \ll \Gamma^*$ (Figure 4a and 4b) correspond to the situation where the strain rate is not large enough to affect the relative fraction of relaxed bonds that re-form as bridges. The overall bridging fraction still decreases in this case, however, because the lifetimes of the load-bearing bridges are less than the lifetimes of the non-load-bearing loops.

Figure 5a displays the predicted flow curve. The stress maximum corresponds to a breakdown of the network structure and is reminiscent of the response predicted by Doi and Edwards[39] for monodisperse polymer melts as well as predictions for physically cross-linked microemulsions,[37] telechelic transient networks,[38] and physical gels.[36] A maximum in the applied stress with increasing strain rate implies that a homogeneous strain field will be unstable and that the solution will tend to separate into shear bands with regions of high and low strain.[10,40,41] At long times, two different shear rates will coexist at the same value of the shear stress. The value of the steady-state stress (σ_∞) was taken as the predicted macroscopic stress at $\gamma = 1000$ for each value of Γ. The range of values predicted for σ_∞ was very similar to the range of large-strain stress values for the experimental data in Figure 3, estimated via extrapolation to $\gamma = 1000$ (note: the stress response at such large strains could not be measured directly due to potential sample aging at the lowest shear rates and sample ejection from the rheometer fixture at the highest shear rates). The flow curve in Figure 5a displays near-Newtonian behavior at low strain rates, followed by regimes of shear thickening and shear thinning, with a stress maximum for $\Gamma/\Gamma^* \sim 0.1$. The nonlinear stress response data displayed in the main plot of Figure 3 for reduced rates of $\Gamma = 0.12-2.4$ corresponds to the shear-thinning regime of Figure 5a.

The predictions from our molecular model shown in Figures 4 and 5 are consistent with the experimental results displayed in Figure 3. The transition from strain stiffening to strain softening, resulting in the stress maxima observed in

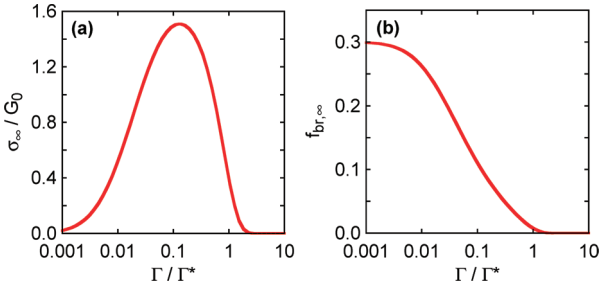

Figure 5. Model predictions for the (a) normalized steady-state stress response and (b) bridging fraction at large strain over a range of normalized reduced rates. The following parameters are used: $f_0 = 0.3$, $\gamma_f = 2.9$, $\Gamma^* = 10$, $\beta = 0.33$, $\gamma = 1000$, and $\gamma^* = 3.7$.

Figure 3, is well captured by the model. Thus, the nonlinear stress response of the deformed physically associating solution is ultimately dependent on the evolution of the macromolecular network structure of the solution, namely shear-induced changes in the bridging fraction. Our model does not predict fracture or shear banding outright, but the main implication of the nonmonotonic flow curve of Figure 5 is that homogeneous shear deformation of the solution will be unstable for large strain rates; thus, we believe that strain localization into shear bands or fracture planes must necessarily evolve in these solutions.

It is worth noting that the rate dependence of the stress response in Figure 3 manifests differently than the constitutive model predictions in Figure 4a, especially at the lowest shear rates. We believe this variation is due to the homogeneous deformation implicit to the constitutive model predictions and the inhomogeneous, *localized* deformation which is believed to be taking place in the solution. As our constitutive model only considers elastic stresses originating from intact strands in the macromolecular network, the existence of flow instabilities will impact the quantitative agreement between the predicted curves (Figure 4) and the experimental data (Figure 3) at intermediate and large values of strain.

Thus, a consequence of our model, where only elastic stresses originating from bridging chains are considered, is that a well-defined fracture plane will emerge, with all of the shear displacement occurring across this plane. Additional dissipative effects, including molecular friction between network chains, clearly need to be accounted for in order to understand the way the system evolves at strains well beyond the strain corresponding to the predicted stress maximum. The occurrence of fracture-like behavior in physically associating solutions can be more directly confirmed by direct visualization of the flow fields during deformation or by comparison to simulations.[10,42] Our triblock copolymer solutions are ideally suited for these investigations because of the wide range of relaxation times and gel strengths that can easily be accessed by simple changes in temperature and polymer concentration.

6. Conclusion

A variety of interesting nonlinear stress responses were found to occur in stress relaxation and shear start-up experiments of model physically associating triblock copolymer solutions. In addition, a constitutive model was developed to elucidate the structural evolution responsible for the observed changes in mechanical response. As the solutions were deformed in shear, strain-stiffening behavior was observed, corresponding to nonlinear stretching of the midblock "bridges" in the macromolecular network. Stiffening was reduced from its predicted elastic limit due to stress relaxation events taking place in the network (i.e., dissociating of bridges from their respective network junctions). Above a critical value of strain, strain-stiffening behavior transitioned to strain softening due to damage accumulation in the network from accelerated strand dissociation and relaxation. This nonlinear behavior was accurately captured by the constitutive model, which incorporated the strain-stiffening behavior of the solution with the strain- and time-dependent evolution of the concentration of intact bridges in the network. Softening was believed to result from the shear-induced formation of highly localized regions of deformation in the macromolecular network. Flow curves predicted from the constitutive model were nonmonotonic, consistent with the onset of flow instabilities at high shear rates.

Acknowledgment. This work was supported through the National Science Foundation through Grant CMMI-0900586. An NSF Graduate Research Fellowship to K.A.E. is also acknowledged, as is the use of facilities provided by the Northwestern University Materials Research Center through the NSF MRSEC program (DMR-0520513).

References and Notes

(1) Seitz, M. E.; Martina, D.; Baumberger, T.; Krishnan, V. R.; Hui, C. Y.; Shull, K. R. *Soft Matter* **2009**, *5*, 447–456.
(2) Gladden, J. R.; Belmonte, A. *Phys. Rev. Lett.* **2007**, *98*, 224501.
(3) Tabuteau, H.; Mora, S.; Porte, G.; Abkarian, M.; Ligoure, C. *Phys. Rev. Lett.* **2009**, *102*, 155501.
(4) Tabuteau, H.; Ramos, L.; Nakaya-Yaegashi, K.; Imai, M.; Ligoure, C. *Langmuir* **2009**, *25*, 2467–2472.
(5) Ravindranath, S.; Wang, S. Q.; Ofechnowicz, M.; Quirk, R. P. *Macromolecules* **2008**, *41*, 2663–2670.
(6) Helgeson, M. E.; Reichert, M. D.; Hu, Y. T.; Wagner, N. J. *Soft Matter* **2009**, *5*, 3858–3869.
(7) Berret, J. F.; Séréro, Y.; Winkelman, B.; Calvet, D.; Collet, A.; Viguier, M. *J. Rheol.* **2001**, *45*, 477–492.
(8) Sprakel, J.; Spruijt, E.; van der Gucht, J.; Padding, J. T.; Briels, W. J. *Soft Matter* **2009**, *5*, 4748–4756.
(9) Berret, J. F.; Séréro, Y. *Phys. Rev. Lett.* **2001**, *87*, 048303.
(10) Hu, Y. T.; Palla, C.; Lips, A. *J. Rheol.* **2008**, *52*, 379–400.
(11) Tixier, T.; Tabuteau, H.; Carriere, A.; Ramos, L.; Ligoure, C. *Soft Matter* **2010**, *6*, 2699–2707.
(12) Schoch, A. B. PhD. Dissertation, Northwestern University, 2009.
(13) Seitz, M. E.; Burghardt, W. R.; Faber, K. T.; Shull, K. R. *Macromolecules* **2007**, *40*, 1218–1226.
(14) Erk, K. A.; Henderson, K. J.; Shull, K. R. *Biomacromolecules* **2010**, *11*, 1358–1363.
(15) Inomata, K.; Nakanishi, D.; Banno, A.; Nakanishi, E.; Abe, Y.; Kurihara, R.; Fujimoto, K.; Nose, T. *Polymer* **2003**, *44*, 5303–5310.
(16) Drzal, P. L.; Shull, K. R. *Macromolecules* **2003**, *36*, 2000–2008.
(17) Bras, R. E.; Shull, K. R. *Macromolecules* **2009**, *42*, 8513–8520.
(18) Baumberger, T.; Caroli, C.; Martina, D. *Nature Mater.* **2006**, *5*, 552–555.
(19) Kumar, S. K.; Douglas, J. F. *Phys. Rev. Lett.* **2001**, *87*, 188301.
(20) Tanaka, F. *Polym. J.* **2002**, *34*, 479–509.
(21) Palmer, R. G.; Stein, D. L.; Abrahams, E.; Anderson, P. W. *Phys. Rev. Lett.* **1984**, *53*, 958–961.
(22) Séréro, Y.; Jacobsen, V.; Berret, J. F.; May, R. *Macromolecules* **2000**, *33*, 1841–1847.
(23) Hotta, A.; Clarke, S. M.; Terentjev, E. M. *Macromolecules* **2002**, *35*, 271–277.
(24) Stukalin, E. B.; Douglas, J. F.; Freed, K. F. *J. Chem. Phys.* **2008**, *129*, 094901.
(25) Gurtovenko, A. A.; Gotlib, Y. Y. *J. Chem. Phys.* **2001**, *115*, 6785–6793.
(26) Skrzeszewska, P. J.; Sprakel, J.; de Wolf, F. A.; Fokkink, R.; Stuart, M. A. C.; van der Gucht, J. *Macromolecules* **2010**, *43*, 3542–3548.
(27) Koga, T.; Tanaka, F.; Kaneda, I.; Winnik, F. M. *Langmuir* **2009**, *25*, 8626–8638.
(28) Berret, J. F.; Roux, D. C.; Porte, G. *J. Phys. II* **1994**, *4*, 1261–1279.
(29) Berret, J. F. *Langmuir* **1997**, *13*, 2227–2234.

(30) Berret, J. F.; Porte, G. *Phys. Rev. E* **1999**, *60*, 4268–4271.
(31) Berret, J. F. In *Molecular Gels: Materials with Self-Assembled Fibrillar Networks*; Weiss, E. G., Terech, P., Eds.; Springer: The Netherlands, 2006; pp 667−720.
(32) Tripathi, A.; Tam, K. C.; McKinley, G. H. *Macromolecules* **2006**, *39*, 1981–1999.
(33) Zhou, J.; Fung, Y. C. *Proc. Natl. Acad. Sci. U.S.A.* **1997**, *94*, 14255–14260.
(34) Lin, D. C.; Douglas, J. F.; Horkay, F. *Soft Matter* **2010**, *6*, 3548–3561.
(35) Seitz, M. E.; Rottsolk, R. L.; Shull, K. R. *J. Polym. Sci., Part B: Polym. Phys.* **2010**, *48*, 1395–1408.
(36) Tanaka, F.; Edwards, S. F. *J. Non-Newtonian Fluid Mech.* **1992**, *43*, 247–271.
(37) Michel, E.; Appell, J.; Molino, F.; Kieffer, J.; Porte, G. *J. Rheol.* **2001**, *45*, 1465–1477.
(38) Sprakel, J.; Spruijt, E.; Cohen Stuart, M. A.; Besseling, N. A. M.; Lettinga, M. P.; van der Gucht, J. *Soft Matter* **2008**, *4*, 1696–1705.
(39) Doi, M.; Edwards, S. F. *The Theory of Polymer Dynamics*; Oxford University Press: Oxford, 1986.
(40) Olmsted, P. D. *Rheol. Acta* **2008**, *47*, 283–300.
(41) Spenley, N. A.; Cates, M. E.; McLeish, T. C. B. *Phys. Rev. Lett.* **1993**, *71*, 939–942.
(42) Manneville, S. *Rheol. Acta* **2008**, *47*, 301–318.